American Mineralogist, Volume 76, pages 1261–1278, 1991

Eruptive pegmatite magma: Rhyolite of the Honeycomb Hills, Utah

ROGER D. CONGDON*
Department of Earth and Planetary Sciences, Johns Hopkins University, Baltimore, Maryland 21218, U.S.A.
W. P. NASH
Department of Geology and Geophysics, University of Utah, Salt Lake City, Utah 84112-1183, U.S.A.

ABSTRACT

The Honeycomb Hills rhyolite represents differentiation in a highly evolved magma. A pyroclastic sequence 12.5 m thick and a dome of ~0.2 km³ occur in western Utah in a region populated with several Tertiary topaz rhyolites. Phenocrysts consist of quartz, sanidine, and albite (10–50% total) in a glassy or fine-grained groundmass. Primary phenocrysts and megacrysts of topaz and fluorsiderophyllite (~1% total) and accessory phases usually associated with rare-element pegmatites occur: fergusonite, ishikawaite, columbite, fluocerite, thorite, monazite, and zircon. Whole-rock composition (SiO_2 = 73.3%, TiO_2 = 0.01, Al_2O_3 = 14.0, Fe_2O_3 = 0.28, FeO = 0.55, MnO = 0.07, MgO < 0.01, CaO = 0.42, Na_2O = 4.59, K_2O = 4.44, P_2O_5 < 0.01, F = 0.61, Cl = 0.10, and maximum values Rb = 1960 ppm, Cs = 78, Li = 344, Sn = 33, Be = 80, and Y = 156) is peraluminous, highly evolved, and comparable to rare element pegmatites. Elevated F contents of up to 2.3% in glass account for low silica and high alumina contents because the granite minimum shifts toward the Ab apex of the Q-Ab-Or ternary with increasing F. Mineralogy and distribution of trace elements with order of eruption indicate evacuation of a cool (570–610 °C), chemically stratified magma chamber. Chemical variation within the erupted volume can be modeled by Rayleigh fractionation of 75% of the phenocryst phases. Spatial variation of some elements, notably Li, Be, B, F, and Cs, may be due to volatile transfer. Enrichment of H_2O and F in interstitial melt during crystallization reduced viscosity enough to allow eruption of the highly crystalline lava of the dome.

INTRODUCTION

The Honeycomb Hills in west-central Utah are the product of a single eruptive cycle of unusual lavas. The lavas are silicic, contain high concentrations of F, are crystal rich, were erupted at low temperature, and contain a suite of unusual accessory minerals. The parent magma was the result of extensive differentiation and was compositionally zoned. High silica concentration and crystal content together with low temperatures would normally mitigate against eruption. The lavas of the Honeycomb Hills provide an opportunity to examine these unusual features, to assess their effects on eruption of the lavas, and to place constraints on differentiation mechanisms in highly evolved silicic magmas. In addition, these lavas are a rare example of an eruptive pegmatite magma, and they provide specific information on crystal-liquid relations in such magmas that are not obtainable from pegmatites themselves.

GEOLOGIC SETTING

The lavas of the Honeycomb Hills were erupted at 4.7 Ma in the eastern Basin and Range province (Lindsey, 1977; Turley and Nash, 1980). Figure 1 is a geologic map of the Honeycomb Hills. Previously, the rhyolite body was considered to be the remains of two or possibly three lava domes (McAnulty and Levinson, 1964; Christiansen et al., 1986). However, flow banding orientations reveal that the Hills are the eroded remnants of a single dome that emanated from a central conduit that can be distinguished by concentric vertical flow banding in coarsely crystalline rhyolite (Congdon and Nash, 1988). There are several other volcanic units in the immediate vicinity, but all are older and unrelated to the genesis of the Honeycomb Hills magma body. An underlying tuff (Ttrt) is similar in composition to tuffs erupted from the Thomas Range 50 km to the east and dated at 6.1 Ma (Turley and Nash, 1980). Latites and dacites of Oligocene age (Hogg, 1972) outcrop adjacent to the Honeycomb Hills and are underlain by the Kalamazoo Tuff dated at 34 Ma (Hagstrum and Gans, 1989). The Kalamazoo Tuff (Tjt) lies unconformably on the Devonian Guilmette Formation, a thick carbonate sequence that overlies about 5 km of lower Paleozoic sediments (Hintze, 1988).

The rhyolites of the Honeycomb Hills can be conveniently divided into two units, a pyroclastic sequence and the overlying lavas that form a dome. The proximal pyroclastic sequence consists of 12.5 m of pumice-bearing air-fall tuffs with rare interbedded surge deposits. The tephra deposit is capped by a vitrophyric breccia that

* Present address: U.S. Geological Survey, M.S. 956, Reston, Virginia 22092, U.S.A.

0003–004X/91/0708–1261$02.00

represents a vitric bomb bed marking the end of the explosive phase of the eruption. The upper unit is a flow-banded felsite that forms the single dome; based upon a present day extent and height (240 m), it had an original volume of approximately 0.2 km³. Any original pumiceous carapace has been lost to erosion that has exposed the internal structure of the dome including the central conduit.

Analytical methods

Whole-rock SiO_2, Al_2O_3, CaO, Fe_{tot}, TiO_2, MnO, Cl, Rb, Y, Zr, and Nb were measured by X-ray fluorescence spectroscopy. MgO and Fe^{2+} were determined volumetrically, P_2O_5 by colorimetry, Na_2O and K_2O by flame photometry, Li by atomic absorption, and F by selective ion electrode. Be, B, As, Cs, Th, U, and rare earth elements (REE) were determined by instrumental neutron activation analysis (INAA) by Neutron Activation Services, Toronto, Canada. Electron microprobe analyses were performed with Applied Research Laboratories EMX-SM and Cameca SX-50 instruments at the University of Utah, using a combination of natural minerals and synthetic materials as standards and applying ZAF and $\phi(\rho z)$ (PAP) correction procedures. Mineral separates of biotite, plagioclase, sanidine, topaz, and quartz were analyzed for trace elements by INAA. Separation was by use of heavy liquids and a Franz isodynamic magnetic separator. Separates were examined under a binocular microscope, and foreign grains were removed by hand. Small accessory minerals were not always eliminated, as discussed below. Modal analyses were made by point counting of samples in thin section. The total number of points counted varied between 1000 and 2000, depending on sample size.

Petrography

The proximal stratigraphic section is illustrated in Figure 2, in which the pyroclastic section is shown to scale. Pyroclastic deposits are light colored (white to light gray) when fresh and oxidized to brown or red-brown when weathered. Pumice fragments up to 50 cm in diameter are abundant, comprising at least 50% of the deposit. Latite clasts averaging 10 cm in diameter are present in conformable layers up to 50 cm thick, and these often comprise up to 50% of an individual layer. These lithic-rich layers delineate "throat clearing" episodes in the initial stages of the eruptive cycle. Other xenoliths include quartzite and limestone clasts up to 50 cm in diameter. Two distinct varieties of quartzite occur as xenoliths. The dome contains red, hematite-stained, slightly conglomeratic quartzite derived from the Prospect Mountain Quartzite of lower Cambrian age. Within the tephra are xenoliths of white quartzite from either the Eureka Quartzite (Ordovician) or sandstone lenses in the Guilmette Formation (Devonian). The Guilmette Formation outcrops a few kilometers west of the Honeycomb Hills. Based on stratigraphic sections for the adjacent Fish Springs and southern Deep Creek Range (Hintze, 1988),

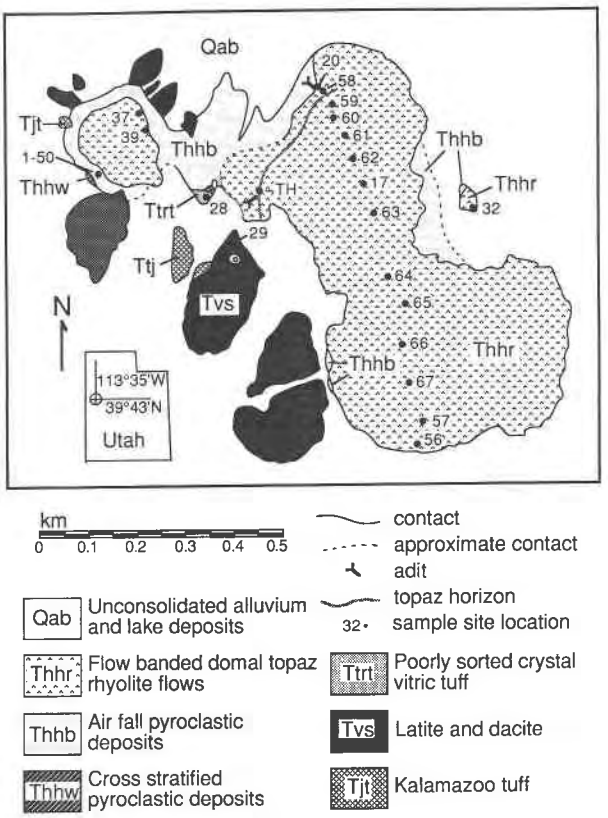

Fig. 1. Geologic map of the Honeycomb Hills area. Location is approximately 113°35′W, 39°43′N. For complete key to the pyroclastic section, see Figure 2.

the Eureka and Prospect Mountain Quartzites lie at depths of about 1 and 5 km, respectively, below the Honeycomb Hills. Pumice fragments contain from 10 to 25% phenocrysts consisting of plagioclase, sanidine, quartz, and less abundant F-rich annite and topaz set in a glassy groundmass (Table 1). Feldspar phenocrysts are euhedral, whereas quartz is commonly embayed and subhedral.

The dome-forming felsites are markedly flow banded, light gray in color when fresh, and brown when weathered. They are holocrystalline, with phenocryst contents ranging from 30 to 40% that consist of sanidine, plagioclase, quartz, biotite, and topaz in decreasing order of abundance (Table 1). The average grain size of the crystalline groundmass is 0.3 mm; groundmass topaz occurs as needles up to 0.1 mm in length. Xenoliths of quartzite up to 50 cm in diameter are present in the dome. Cognate (?) xenoliths of pegmatite up to 20 cm in diameter and topaz-rich xenoliths are present. The pegmatite xenoliths contain miarolitic cavities and are composed of potassium feldspar, plagioclase, quartz, biotite, and topaz, typically 1–2 cm in diameter. Topaz-rich xenoliths are poikilitic in texture and contain up to 20% topaz together with quartz, potassium feldspar, plagioclase, and fluorite. Megacrysts of topaz, sanidine, and biotite are common in a zone denoted "Topaz Horizon" in Figure 1. This is a horizon approximately 10–20 m thick and subparallel

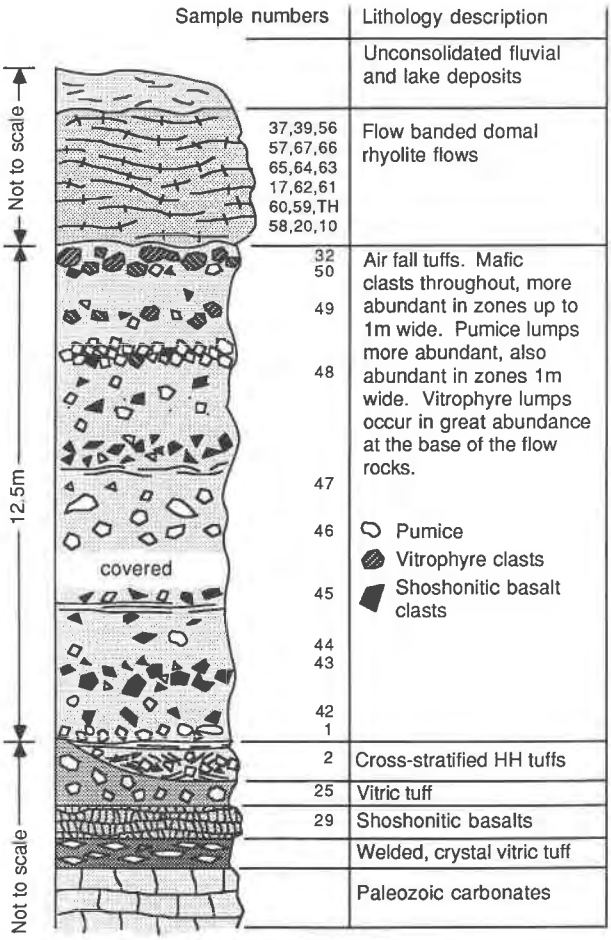

Fig. 2. Stratigraphic column of the Honeycomb Hills area. Only the tephra section is to scale.

to flow banding. Megacryst sizes are: sanidine, 1–3 cm typical, up to 8 cm; topaz, up to 3 cm; and biotite, up to 2 cm. Vugs and lithophysae, evidence of a discrete vapor phase, are not present in the dome felsite.

Magnetite is more abundant in the pyroclastic sequence but is still present only in trace amounts; it is commonly oxidized. Other trace phases in both units include zircon, thorite, monazite, fluorite, fluocerite, columbite, fergusonite, and ishikawaite.

Mineralogy

Quartz

Phenocrysts of quartz are smokey throughout but appear to be less often embayed in felsite than in pumice. Neutron activation analyses of quartz separates are given in Table 2. Quartz contains trace amounts of transition metals but in lesser amounts than coexisting sanidine. U and Th are at the 2 ppm level. Some quartz grains contain melt inclusions that may be responsible for those trace elements as well as the 400 ppm Na reported; Na could also be present to balance charge for trace amounts of Al, which is usually present in quartz.

Feldspar

Sanidine and plagioclase (Ab_{93-98}) occur as phenocrysts and in the groundmass. Sanidine phenocrysts are typically 1–3 mm in diameter, and plagioclase is usually 0.5–1 mm. Feldspars of both varieties are unzoned, euhedral, and without reaction rims.

Chemical analyses are given for feldspar in Table 3. Average mole percent compositions are $An_6Ab_{88}Or_6$ for plagioclase and $An_{0.3}Ab_{32}Or_{68}$ for sanidine, with little difference between feldspars from pumice or felsite except that the most Ab-rich plagioclase occurs in pumice. All Honeycomb Hills plagioclase is more sodic (Ab_{85-95}) than plagioclase reported for Macusani glass (Ab_{83-84}) (Pichavant et al., 1987) or other rhyolite localities in the western United States.

Plagioclase exhibits a negative Eu anomaly (Fig. 3), although Eu in oligoclase was below the limit of detection (0.05 ppm). On chondrite-normalized diagrams, plagioclase is normally enriched in Eu relative to the other REE (Drake and Weill, 1975; Nash and Crecraft, 1985). Three

Table 1. Modal analyses (vol%)

	Pumice				Vitro-phyre	Felsite								Peg-matite xenolith
	1	45	46	48	32	20	58	TH	59	60	62	17	63	10
Phenocrysts														
Sanidine	2.34	2.93	8.79	6.84	15.21	18.90	15.78	13.80	18.34	14.99	20.29	16.20	20.68	16.92
Plagioclase	3.76	4.13	5.74	9.52	10.71	7.22	9.53	12.70	10.12	12.99	9.43	11.30	12.09	6.46
Quartz	2.85	1.60	4.95	10.09	12.41	4.62	8.46	13.50	7.52	7.99	7.72	9.36	6.52	53.30
Biotite	tr.	0.41	0.75	0.52	0.73	0.66	0.68	1.29	1.46	1.62	0.76	0.32	0.63	3.18
Topaz	tr.	tr.	tr.	tr.	tr.	tr.	tr.	0.66	tr.	tr.	tr.	0.09	tr.	19.58
Fluorite	tr.	tr.	0.15	tr.	tr.	tr.	0.15	tr.	tr.	tr.	tr.	tr.	tr.	tr.
Opaques	tr.	tr.	tr.	tr.	0.20	tr.	tr.	0.15	tr.	0.15	0.14	0.32	0.15	tr.
Total	8.95	9.07	20.38	26.97	39.26	31.40	34.59	42.10	37.45	37.74	38.33	37.59	40.07	99.44
Groundmass														
Glass	59.93	70.10	57.01	59.54	60.74									
Voids	31.12	20.83	22.60	13.49										
Undifferentiated						68.60	65.41	57.90	62.55	62.26	61.67	62.41	59.93	
Total	100.0	100.0	100.0	100.0	100.0	100.0	100.0	100.0	100.0	100.0	100.0	100.0	100.0	99.4

Note: Mode for sample 10X was calculated by least-squares fit of whole-rock data to analyses of phases present.

TABLE 2. Neutron activation analyses of mineral separates

	Pumice		Vitrophyre					Megacrysts		
	1 Bi	48 Bi	32 Bi	32 Pg	32 Sa	32 Qz	32 Tz	TH Bi	TH Tz	TH Sa
Sc	120	134	114	0.16	0.17	0.12	5.10	141	0.78	0.15
Co	4.7	4.4	4.0	1.1	1.1	0.7	0.7	2.6	1.1	1.5
Zn	500	720	420	13	13	6	28	440	17	26
As	4	6	2	<1	<1	<1	3	20	<1	<1
Br	*	*	*	*	*	*	*	14	10	10
Rb	4500	4300	3600	30	1200	<10	110	6100	<10	4700
Sb	18.0	8.4	5.9	0.8	1.3	0.9	1.5	8.6	1.5	1.7
Cs	44.0	36.9	32.8	0.8	2.0	0.3	4.9	78.2	0.5	9.2
Ba	150	150	340	<20	20	20	990	<20	<20	50
Hf	5.2	13	18	1.4	0.9	0.8	27	1.2	<0.2	<0.2
Ta	91	92	87	0.6	0.5	<0.5	28	240	0.7	<0.5
W	24	10	25	<1	<1	<1	20	31	<1	<1
Au (ppb)	9	<5	14	<5	<5	5	6	9	290	<5
Th	11	25	82	6.3	2.7	2.2	85	3.0	<0.2	<0.2
U	23.1	30.5	78.0	3.3	2.1	2.1	68.2	34.2	0.1	0.2
La	14.2	31.8	67.3	34.4	14.3	2.3	482.0	6.0	0.3	0.8
Ce	55	166	263	59	17	6	1210	<1	1	1
Nd	6	21	44	9	3	<3	336	<3	<3	<3
Sm	3.55	8.53	19.60	1.61	0.49	0.47	60.6	<0.01	<0.01	0.02
Eu	0.20	0.27	0.13	<0.05	0.11	0.06	0.14	<0.17	0.10	0.10
Tb	0.8	2.8	6.4	0.3	0.1	0.2	9.4	<0.2	<0.1	<0.1
Yb	9.91	27.1	62.7	2.12	1.33	1.4	92.7	0.41	0.1	<0.05
Lu	2.10	4.82	11.20	0.40	0.29	0.28	16.1	0.13	0.01	<0.01

Note: Samples 1T Bi through 32V Tz are phenocrysts. Samples TH Bi through TH Sa are from single megacrysts. Values in ppm. Bi = biotite, Pg = plagioclase, Sa = sanidine, Qz = quartz, Tz = topaz.

* Data unusable because of the use of bromoform in separation techniques.

factors promote low concentrations of Eu in feldspar at the Honeycomb Hills: (1) the Honeycomb Hills magma was at a relatively oxidizing condition (see below), increasing the proportion of Eu^{3+}, (2) partition coefficients for Eu decrease with decreasing anorthite content in plagioclase (Nash and Crecraft, 1985), and (3) the Honeycomb Hills magma has very low concentrations of Eu, often below the detection limit.

Sanidine is the only phenocryst phase without a large negative Eu anomaly. The K_d for Eu is much higher than for adjacent REE (0.48 for Eu, 0.04 for Sm, and 0.04 for Tb), although it remains less than 1. Reducing the albite

TABLE 3. Representative analyses of feldspar

Sample	1	42	43	45	46	47	48	32	20	TH	60	61	56	10
							Alkali feldspar							
SiO_2	66.2	66.1	65.7	65.4	65.7	65.5	65.2	66.1	65.5	65.8	65.7	66.1	65.3	65.7
Al_2O_3	18.8	18.7	18.6	18.5	18.5	18.5	18.6	18.8	18.5	18.6	18.5	18.5	18.6	18.6
Fe_2O_3	0.04	0.04	—	—	0.03	0.04	0.06	—	—	0.04	—	—	0.03	—
CaO	0.04	0.04	0.02	0.04	0.02	0.02	0.06	0.05	0.03	0.05	0.06	0.05	0.04	—
BaO	—	0.03	—	—	—	—	—	—	—	—	—	—	—	—
Na_2O	3.47	3.42	3.44	3.39	3.58	3.46	3.52	3.74	3.53	3.76	3.86	3.77	3.76	3.06
K_2O	11.8	11.8	11.9	11.9	11.8	11.8	11.7	11.4	11.8	11.4	11.3	11.4	11.4	12.4
Rb_2O	0.10	0.11	0.15	0.12	0.14	0.11	0.07	0.09	0.13	0.09	0.07	0.09	0.10	0.20
Total	100.4	100.2	99.8	99.4	99.8	99.4	99.2	100.2	99.5	99.7	99.5	99.9	99.2	100.0
Ab	30.8	30.4	30.4	30.1	31.5	30.8	31.3	33.1	31.1	33.3	34.0	33.5	33.4	27.3
Or	69.0	69.4	69.5	69.7	68.4	69.1	68.4	66.7	68.7	66.4	65.7	66.2	66.4	72.7
An	0.2	0.2	0.1	0.2	0.1	0.1	0.3	0.2	0.2	0.3	0.3	0.3	0.2	0
							Plagioclase							
SiO_2	67.0	67.3	67.8	67.0	66.9	66.4	66.5	66.9	66.8	66.6	66.7	66.7	67.1	67.9
Al_2O_3	20.9	20.6	19.9	20.4	20.3	20.2	20.7	20.6	20.4	20.3	20.8	20.2	20.5	20.1
Fe_2O_3	—	—	—	—	0.03	0.06	—	0.05	0.04	0.04	—	—	—	0.04
CaO	1.50	1.26	0.68	1.43	1.28	1.25	1.61	1.40	1.38	1.31	1.66	1.25	1.29	0.57
BaO	—	—	—	—	—	—	—	—	—	—	—	—	—	—
Na_2O	10.2	10.5	10.7	10.2	10.3	10.3	10.2	10.1	10.2	10.1	10.0	10.3	10.3	11.1
K_2O	0.97	0.89	0.93	0.92	1.08	1.00	0.95	1.10	1.08	1.11	0.98	1.02	1.05	0.38
Rb_2O	—	—	—	—	—	—	—	—	—	—	—	0.03	—	—
Total	100.6	100.5	100.0	100.0	100.0	99.2	100.0	100.2	99.9	99.5	100.1	99.5	100.2	100.1
Ab	87.4	89.1	91.6	87.9	87.9	88.4	87.0	87.2	87.3	87.5	86.5	88.3	88.0	95.2
Or	5.5	5.0	5.2	5.2	6.1	5.7	5.4	6.1	6.1	6.3	5.6	5.8	5.9	2.1
An	7.1	5.9	3.2	6.9	6.0	5.9	7.6	6.7	6.6	6.2	7.9	5.9	6.1	2.7
T (°C)*	577	589	573	580	558	567	610	592	583	621	603	619	584	(524)**

Note: Dash = concentration < 0.03. End-members in mol%.

* Two-feldspar convergence temperature at 1 kbar pressure (Fuhrman and Lindsley, 1988).

** AB temperature—no convergence.

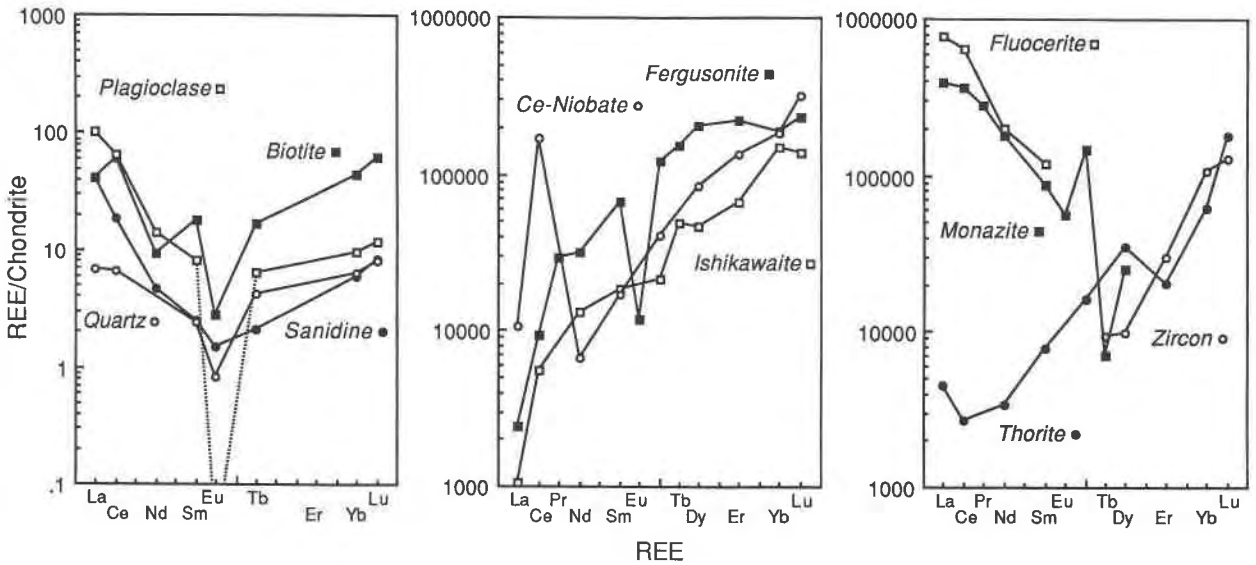

Fig. 3. Chondrite-normalized plots of REE for phenocrysts and accessory minerals. Feldspar, biotite, and quartz data are by INAA; accessory phases were analyzed by electron microprobe. Eu value for plagioclase is maximum possible (= detection limit).

component of sanidine apparently reduces the Eu content (Nash and Crecraft, 1985), although the effect is not as pronounced as reducing anorthite in plagioclase.

Mica

The mica of the Honeycomb Hills occurs as phenocrysts up to 1 mm in diameter throughout the eruptive sequence and as megacrysts in the topaz horizon of the dome. The mica is unusual in composition because it is extraordinarily enriched both in Fe and F. The high F content of the iron mica attests to the abnormally high f_{HF}/f_{H_2O} ratio present in the magma, as discussed below.

Analyses of representative mica samples are presented in Table 4. Structural formulas are calculated on the basis of 22 O atoms; H_2O content is calculated from stoichiometry of the OH-halogen site. The micas contain substantial $^{[6]}Al$ and less than six cations in the octahedral site, resulting in some dioctahedral character. The composition closely approximates siderophyllite (Deer et al., 1962). Two separates analyzed for Li contained 0.1% Li, insufficient to fill the octahedral site. The significant difference between biotite samples in the pyroclastic sequence and in the dome is that the former contain less than 3% F, whereas the latter average over 5% F with some individual grains containing as much as 7.5% F. In other respects, the mica samples are of similar composition, with domal biotite containing slightly more Rb and Mn and less Fe. A detailed description of Honeycomb Hills micas is in preparation.

Topaz

Topaz is common throughout the Honeycomb Hills lavas in concentrations up to 0.6 vol%. The topaz is near end-member fluortopaz with 20 wt% F. In the typical topaz rhyolites of the eastern Basin and Range province, topaz forms by crystallization from the vapor phase in cavities in felsite. At the Honeycomb Hills, topaz is a primary phenocryst phase. Altogether three generations of topaz are present: megacrysts up to 3 cm in diameter, phenocrysts up to 0.5 mm, and abundant needles up to 0.1 mm in the groundmass of the felsite. Most topaz is euhedral with well-developed terminations and (110) and (210) prisms (Fig. 4). Coprecipitation with mica is indicated by inclusion of each in phenocrysts of the other. Phenocrysts of topaz also contain inclusions of plagioclase, sanidine, quartz, zircon, monazite, and columbite.

Fluorides

Primary fluorite occurs as euhedral microphenocrysts of 5–20 μm in diameter in pumice and vitrophyre. Fluorite also occurs in anhedral masses up to 1 mm in diameter in the groundmass of some domal felsites and at the contact between the top of the pyroclastic section and the base of the dome, where it has been concentrated by hydrothermal processes.

Fluocerite [$(Ce,La)F_3$] occurs as euhedral microphenocrysts, 10–50 μm in length in vitrophyre, and as small (<0.1 mm) inclusions in phenocryst biotite in felsite of the topaz horizon. Light rare earths and F predominate in this mineral (Table 5). The usual occurrence of fluocerite is in rare element pegmatites (Henderson, 1984), and we believe this to be the first occurrence of fluocerite in an extrusive rock.

Orthosilicates

Zircon occurs as 5–50 μm diameter microphenocrysts and as inclusions in mica and niobates. It occasionally contains micrometer-size inclusions of thorite.

Thorite occurs as discrete grains, 2–10 μm in diameter, associated with zircon and as inclusions from micrometer

Table 4. Average microprobe analyses of biotite

	Pumice	Vitrophyre		Dome
Sample	1	32	20	60
SiO_2	34.3	33.8	36.2	36.1
TiO_2	0.42	0.68	0.47	0.77
SnO_2	0.06	0.05	0.06	0.04
Al_2O_3	19.2	19.0	19.6	18.1
FeO	31.9	32.1	26.3	26.4
MnO	0.97	0.73	1.17	1.90
MgO	0.09	0.14	0.12	0.24
CaO	—	—	0.04	—
Na_2O	0.36	0.40	0.77	0.43
K_2O	9.0	9.0	8.7	8.9
Rb_2O	0.37	0.30	0.59	0.55
F	2.91	2.73	5.13	5.61
Cl	0.19	0.31	0.18	0.27
H_2O	2.31	2.34	1.27	0.97
Sum	102.1	101.6	100.5	100.2
−O = F,Cl	−1.26	−1.22	−2.20	−2.42
Total	100.8	100.4	98.3	97.8
Si	5.50	5.46	5.79	5.86
$^{[4]}$Al	2.50	2.54	2.21	2.14
Sum tet:	8	8	8	8
$^{[6]}$Al	1.14	1.08	1.49	1.31
Ti	0.05	0.08	0.06	0.09
Sn	0	0	0	0
Fe	4.28	4.34	3.52	3.58
Mn	0.13	0.1	0.16	0.26
Mg	0.02	0.03	0.03	0.06
Sum oct:	5.62	5.63	5.26	5.3
Na	0.11	0.13	0.24	0.14
K	1.84	1.85	1.78	1.83
Ca	0	0	0	0
Rb	0.04	0.03	0.06	0.06
Sum int:	1.99	2.01	2.08	2.03
OH	2.47	2.52	1.35	1.05
F	1.48	1.39	2.6	2.88
Cl	0.05	0.09	0.05	0.07
Sum hyd:	4.00	4.00	4.00	4.00
*X*Mg*	0.004	0.006	0.005	0.011
*X*Sid*	0.85	0.85	0.81	0.74
*X*Ann*	0.15	0.15	0.18	0.25
$\log[f_{H_2O}/f_{HF}]$**	2.86	2.9	2.37	2.24
f_{H_2O}†	1001	1135	200	133
f_{HF}	1.4	1.4	0.9	0.8
IV(F)**	0.45	0.49	−0.1	−0.16

* *X*Mg, *X*Sid, *X*Ann = mole fraction end-members from Munoz (1984).
** From Munoz (1984).
† From Equation 1 in text.

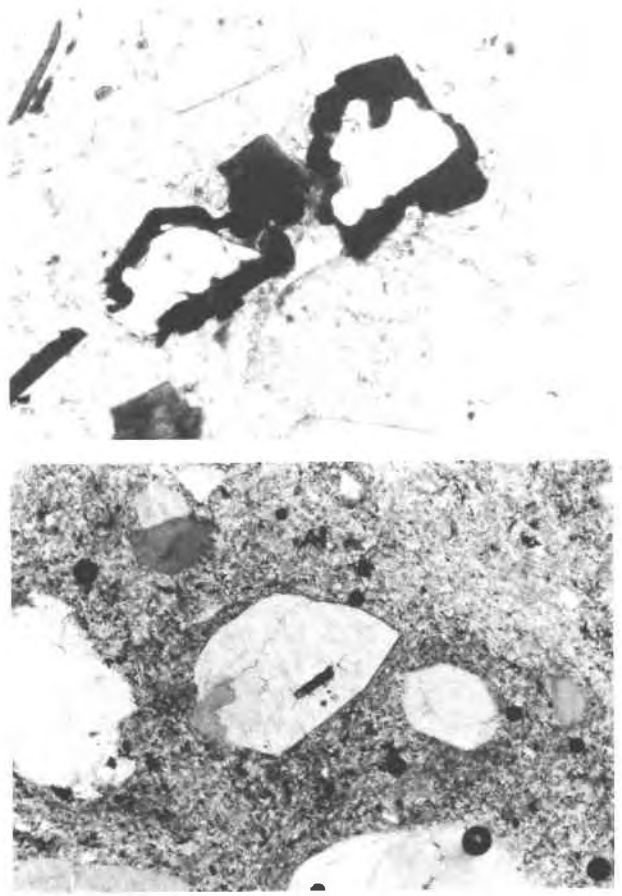

Fig. 4. Photo micrographs of topaz inclusions in biotite (sample 32, upper photograph) and a biotite inclusion in topaz (sample 62, lower photograph). Upper photograph is approximately 2 mm across; lower is approximately 1.5 mm.

to submicrometer size in zircon. Both zircon and thorite contain substantial U, and both preferentially incorporate heavy REE (Fig. 3).

Niobates

Columbite [(Fe,Mn)$(Nb,Ta)_2O_6$] occurs as microphenocrysts (2–10 μm in length) in vitrophyre, in the groundmass of felsites, and as inclusions in biotite and topaz; in several instances, it occurs in growth contact with ishikawaite. Unlike the other coexisting niobates, columbite does not incorporate REE or actinides; it does contain more Ta and Mn than coexisting niobates (Table 5).

Fergusonite [an yttrium niobate (Y,Ca,Ce,U,Th)(Nb,Ta,-Ti)O_4], ishikawaite [a U-rich variety of samarskite (Y,Ce,U,Fe)$(Nb,Ta,Ti)_2(O,OH)_6$], and an unknown Ce-niobate occur as euhedral, prismatic microphenocrysts up to 50 μm in diameter in vitrophyre and as inclusions in biotite. These three niobates contain substantial amounts of the heavy rare earths and, collectively, high concentrations of U, Th, Nb, Ta, and Y (Table 5; Fig. 3).

Phosphate

Monazite occurs as inclusions 5–20 μm in diameter in biotite and topaz phenocrysts, often in association with zircon and thorite. Monazite contains substantial Th in addition to light REE.

Composition of Lavas

Major elements

SiO_2 contents for rhyolites of the Honeycomb Hills range from 70.4 wt% (72.5%, anhydrous) in pumice to 76.3% in domal felsites and from 70.1 to 71.9% in glasses normalized to an anhydrous composition (Table 6). By comparison, SiO_2 contents range from 73.0 to 76.5% in rhyolite from Spor Mountain, Utah, the closest analogue in composition to the Honeycomb Hills (Christiansen et al., 1984). On average, silica contents in Honeycomb Hills are lower than those of less evolved silicic systems in the

TABLE 5. Microprobe analyses of representative accessory minerals

	A	B	C	D	E	F	G	H
	Zircon	Thorite	Monazite	Fluocerite	Columbite	Fergusonite	Ishikawaite	Cerium niobate
SiO_2	30.1	18.4	3.13					
TiO_2					1.25	0.79	0.59	
SnO_2					0.78	—	1.52	
ZrO_2	54.2	0.18	0.43					
HfO_2	5.49	—	0.16					
ThO_2	0.63	47.4	12.6	0.58		1.53	6.39	1.07
UO_2	4.09	24.2	0.48			3.26	23.6	9.27
FeO		0.74			12.20	2.00	9.47	14.20
MnO					7.48	0.03	2.10	2.23
CaO	—		0.10	0.53		0.36	0.11	0.61
P_2O_5	0.41		25.7					
Nb_2O_5					68.1	42.5	39.5	39.3
Ta_2O_5					9.28	1.53	5.13	4.97
Y_2O_3	—	1.48	0.85	0.96	0.18	23.0	1.05	1.62
La_2O_3	—	0.13	11.10	18.80	0.10	0.07	0.03	0.30
Ce_2O_3	—	0.20	27.10	41.40	0.09	0.70	0.41	12.80
Pr_2O_3			2.28			0.33		
Nd_2O_3	—	0.19	9.89	9.55	0.06	1.73	0.73	0.37
Sm_2O_3	—	0.14	1.53	1.81	—	1.20	0.33	0.30
Eu_2O_3	—	—	0.38	—	—	0.08	—	—
Gd_2O_3	—	0.38	3.45	—	—	2.84	0.50	0.96
Tb_2O_3	0.04	—	0.03	—	—	0.66	0.21	—
Dy_2O_3	0.29	1.02	0.73	—	—	6.02	1.37	2.43
Er_2O_3	0.57	0.39	—	—	—	4.15	1.27	2.54
Yb_2O_3	2.00	1.16	—	—	—	3.56	2.87	3.45
Lu_2O_3	0.37	0.52	—	—	—	0.67	0.40	0.92
F		0.19	0.48	25.7		—		0.25
Sum	98.2	96.5	100.5	99.3	99.5	96.9	97.6	96.9
−O = F		0.1	0.2	—		—		0.1
Total	98.2	96.4	100.3	99.3	99.5	96.9	97.6	96.8

Note: A blank value indicates the element was not determined; a dash (—) indicates abundance below the level of detection (approximately 0.03%). A = Zircon inclusion in topaz; topaz horizon felsite TH. B = Thorite microphenocryst; vitrophyre 32. C = Monazite inclusion in biotite phenocryst; vitrophyre 32. D = Fluocerite microphenocryst; vitrophyre 32. Values in % element. E = Columbite inclusion in topaz phenocryst; topaz horizon felsite TH. F = Fergusonite in biotite phenocryst; vitrophyre 32. G = Ishikawaite microphenocryst; vitrophyre 32. H = Cerium niobate microphenocryst; vitrophyre 32.

western United States such as the Bishop Tuff (75.5–77.4%; Hildreth, 1979); Coso, California (73.8–77.0%; Bacon et al., 1981); Thomas Range, Utah (73.3–76.2%); and Smelter Knolls, Utah (73.3–76.2%; Turley and Nash, 1980). However, lower SiO_2 contents of highly evolved magma are consistent with high F contents, as shown experimentally by Manning (1981), in which the ternary minimum in the system quartz-albite-orthoclase shifted toward the feldspar join with increasing content of F (Fig. 5). We believe that whole-rock F contents do not represent initial magma concentrations or F contents at the time of eruption. F has been lost from glassy samples selectively after eruption. Pumices with thin bubble walls contain negligible amounts of F, whereas massive glass in the vitrophyre contains 2.3% F (Table 6). F contents of melt inclusions in quartz phenocrysts range from 3.0 to 3.5% in early erupted pumice to 1 to 3% in domal lavas (Gavigan et al., 1989). These elevated F contents are similar to concentrations reported for ongonites (Kovalenko and Kovalenko, 1976; Kovalenko, 1973; Kovalenko et al., 1971, 1977) and topaz granites (Pichavant and Manning, 1984) and higher than most topaz rhyolites. The results presented in Figure 5 are consistent with the higher F concentrations in the magma volume that gave rise to the pyroclastic sequence than in the mass that was later erupted passively as domal felsites.

The shift in the ternary minimum toward the feldspar join with increasing F results in higher Al and lower silica contents in early erupted pumice than in later erupted felsites. Normative corundum ranges from 0 to 1.5%. The total alkali content decreases through the eruptive sequence with a concomitant decline in the Na_2O/K_2O ratio from 1.7 to 1.2. Fe and Mg do not vary significantly, and Mg, Ti, and P are present in trace amounts; in all cases these elements are less abundant than Rb.

The major element composition of Honeycomb Hills lavas is similar to the peraluminous glass from Macusani, Peru (Pichavant et al., 1987; London et al., 1988) except that Al_2O_3 is lower at Honeycomb Hills (13–15%) vs. the Macusani glass (nearly 16%), which results in higher normative corundum. F contents in vitrophyre are higher at Honeycomb Hills (2.3%) than in Macusani glass (1.3%). Despite these general similarities, there are notable exceptions in the extraordinarily high contents of P_2O_5 (0.53%), B_2O_3 (0.62%), and Li_2O (0.74%) in Macusani glass; these elements are 1–2 orders of magnitude less abundant at the Honeycomb Hills. A second rhyolite that closely resembles Honeycomb Hills rhyolite in compo-

sition is at Spor Mountain, Utah, erupted at 21 Ma 50 km to the east of the Honeycomb Hills (Christiansen et al., 1984). Webster et al. (1987) studied the phase equilibria of this composition, and their results are applicable to the Honeycomb Hills system as described below.

Trace elements

The extreme differentiation of the Honeycomb Hills magma is shown by enrichments in several elements (Table 7). Some maximum values (ppm) are: Rb 1960, Cs 78, Li 344, Sn 33, Be 80, and Y 156. Ti (294 ppm maximum) and Zr (67 ppm maximum) are examples of strongly depleted elements. By comparison, maximum concentrations of incompatible elements in the Bishop Tuff are about $1/10$ those of the Honeycomb Hills: Rb 190, Cs 7.2, Li 37, Sn 3.6, Be 4.1, and Y 25; concentrations of compatible elements are Ti 1260 and Zr 140 (Hildreth, 1979). With respect to the Macusani glass (Pichavant et al., 1987; London et al., 1988), the lavas of the Honeycomb Hills contain more Be, Cl, Sc, Co, Rb, Y, Nb, Sb, Hf, Pb, Th, and REE; the latter are ten to 100 times more abundant at the Honeycomb Hills. Macusani glass is relatively enriched in Zn, As, Sn, Cs, and W. Samples from both localities have similar contents of Zr, Ta, and U and are characterized by very low Sr and Ba.

The systematic variation in elemental abundances with respect to sequence of eruption at the Honeycomb Hills

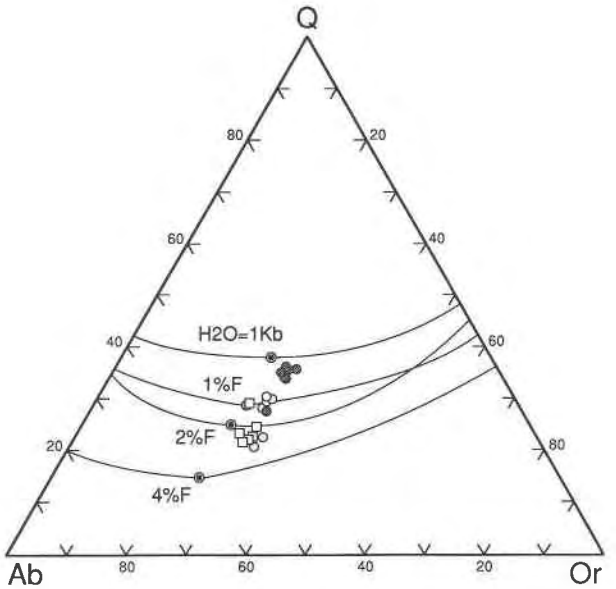

Fig. 5. Quartz-albite-orthoclase ternary with minimum melt compositions for H_2O = 1 kbar, 1% F, 2% F, and 4% F (adapted from Manning, 1981). Filled circles are whole-rock domal felsite, open circles are pumice, and open squares are electron microprobe analyses of glass.

TABLE 6. Representative major element analyses and CIPW norms

	Pumice		Vitrophyre	Felsite			Xenolith	Glass	
	1	43	32	20	TH	66	10	1G	32G
SiO_2	70.7	70.4	73.3	72.8	76.0	76.1	74.9	66.6	66.4
TiO_2	0.01	0.01	0.01	0.01	0.01	0.04	0.03	<0.01	<0.01
Al_2O_3	15.1	15.1	14.0	14.5	13.0	13.0	16.9	15.4	15.5
Fe_2O_3	0.16	0.04	0.28	0.53	0.53	0.93	0.82	0.19	0.05
FeO	0.52	0.55	0.55	0.31	0.36	0.20	0.13	0.34	0.49
MnO	0.09	0.10	0.07	0.07	0.08	0.06	0.07	0.08	0.11
MgO	<0.01	<0.01	<0.01	<0.01	<0.01	<0.01	<0.01	<0.01	<0.01
CaO	0.69	1.10	0.42	1.59	0.44	0.36	1.05	0.35	0.32
Na_2O	4.99	5.25	4.59	4.64	4.11	3.80	1.13	4.87	4.73
K_2O	4.86	4.83	4.44	4.55	4.58	4.92	2.41	4.15	4.31
P_2O_5	<0.01	<0.01	<0.01	0.04	0.01	0.01	0.02	0.18	0.17
F	0.54	0.48	0.61	0.31	0.85	0.56	2.00	0.69	2.36
Cl	0.11	0.10	0.10	0.05	0.03	0.11	n.d.	0.15	0.15
H_2O^+	2.57	1.92	0.80	0.04	0.18	<0.01	1.32	n.d.	n.d.
H_2O^-	0.30	0.40	0.24	0.03	0.02	0.05	0.02	n.d.	n.d.
Sum	100.64	100.28	99.41	99.47	100.20	100.14	100.80	93.0	94.7
−O = F,Cl	0.25	0.22	0.28	0.14	0.36	0.26	0.84	0.32	1.02
Total	100.39	100.06	99.13	99.33	99.84	99.88	99.96	92.6	93.6
SiO_2 (H_2O free):	72.5	72.0	74.7					71.9	70.9
				CIPW normative minerals					
Quartz	21.20	19.00	28.40	25.50	33.50	34.20	56.90	21.3	21.3
Corundum	0.35	—	0.90	—	0.55	0.83	10.60	2.25	2.5
Orthoclase	28.70	26.90	26.20	26.90	27.10	29.10	14.20	24.5	25.5
Albite	42.20	44.40	38.80	39.30	34.80	32.20	9.56	41.20	40.00
Anorthite	3.42	3.23	2.08	5.27	2.12	1.72	5.08	1.74	1.59

Note: Samples 1T through 10X were determined by X-ray fluorescence, flame photometry (for Na_2O and K_2O), select ion electrode (F), sodium tungstate fusion (H_2O^+), and drying overnight at 110 °C (H_2O^-). Samples 1G through 32G are microprobe analyses of glasses in pumices and the vitrophyre (sample 32V). Silica has been shown with analyses normalized to 100% for reference and comparison with whole-rock data. F is ignored in the CIPW calculation; if included, Ca is allocated to CaF_2, resulting in no normative An, which is an inappropriate representation of two feldspar rhyolites. Analyses of other samples are available from the authors.

Table 7. Representative trace element analyses of whole-rock samples

	1G	1	43	32G	32	20	TH	66
Li	n.d.	306	192	n.d.	344	294	242	116
Be	n.d.	79	267	65	68	36	11	—
B	260	190	220	190	130	92	32	28
Cl	n.d.	1060	991	n.d.	1030	537	316	1060
Sc	6.13	6.77	4.84	5.28	4.60	4.38	3.90	3.88
Ti	n.d.	36	52	n.d.	68	49	56	220
Mn	n.d.	733	784	n.d.	571	545	637	494
Co	1.6	1.1	*	1.5	*	*	*	*
Zn	39	59	17	31	25	18	26	29
As	31	25	29	22	14	13	5	5
Br	*	1.2	6.6	*	8.4	3.8	15	4.2
Rb	n.d.	1560	1960	n.d.	1370	1460	1440	1050
Sr	n.d.	21	37	n.d.	8	33	11	14
Y	n.d.	39	51	n.d.	84	85	91	156
Zr	n.d.	27	23	n.d.	47	42	48	67
Nb	n.d.	81	75	n.d.	74	86	84	85
Sn	n.d.	25	33	n.d.	22	23	14	9
Sb	5.7	1.5	5.4	7.7	3.5	2.0	4.9	1.4
Cs	78.4	75.9	75.7	61.4	39.6	34.2	37.0	16.4
Ba	n.d.	58	—	n.d.	—	125	—	—
Hf	5.9	4.3	3.7	6.5	6.0	5.0	5.0	6.2
Ta	44	35	*	32	*	*	*	*
W	34	22	*	25	*	*	*	*
Au (ppb)	15	<5	19	<5	35	6	5	5
Th	19	18	15	22	24	25	24	42
U	29.9	31.8	19.0	26.6	26.1	16.2	18.1	15.4
La	28.8	23.7	16.2	34.6	40.2	38.8	47.7	52.7
Ce	94	95	57	139	139	137	137	155
Nd	18	25	13	28	38	32	35	44
Sm	5.70	5.56	3.08	11.40	10.80	10.40	11.40	14.30
Eu	0.21	0.08	0.24	0.23	<0.05	0.16	0.19	0.13
Tb	1.6	1.3	0.7	2.8	2.6	2.8	3.1	3.7
Yb	19.6	16.2	9.96	31.5	29.1	30.6	31.7	30.4
Lu	3.60	3.03	1.94	5.84	5.22	5.30	5.64	5.03

Note: Values in ppm. Li, Be, and Sn by atomic absorption. Cl, Ti, Mn, Rb, Sr, Y, Zr, Nb, and Ba by X-ray fluorescence. Sc, Co, Zn, As, Br, Sb, Cs, Hf, Ta, W, Au, Th, U, and the REE by instrumental neutron activation analyses. Dash = Not detected; n.d. = not determined.
* Data unusable because of the use of tungsten carbide or bromoform in preparation. Analyses of other samples available from the authors.

is illustrated in Figure 6. Several significant features are evident in the data presented in Figure 6. Collectively, the data illustrate that the eruption tapped a compositionally zoned magma chamber. The least evolved magma occurs in the area of the conduit and is characterized by relative enrichments in Si, K, Ti, Fe, Y, Sr, Th, and REE. The more differentiated magma is relatively enriched in Li, Be, B, Na, Al, Sc, As, Rb, Sn, Cs, and U and was erupted earlier in the volcanic cycle. Analyses of two glass separates show the same compositional trends and demonstrate that these variations are shared by the melt and are not simply a function of changing crystal content. For most elements, there is greater range and fluctuation in concentration within the pyroclastic unit than across the dome. In addition, some elements fluctuate in abundance rather than displaying a progressive change in concentration with order of eruption. This is more pronounced in the tephra than the dome, and we attribute this behavior to the dynamics of the eruption by which compositionally distinct batches of magma may be erupted simultaneously or, during a hiatus in the eruption, unerupted evolved magma may reoccupy the upper reaches of the magma chamber near the conduit (Spera, 1984; Spera et al., 1986).

Contamination by lithic fragments from underlying latite or dacite is evident in the tephra sample at 11 m, which has anomalously high contents of Ti, Mn, and Fe. Whole-rock F contents are variable and do not represent magmatic values; F contents in massive glass and melt inclusions range from 2.3 to 3.5%. The extent to which individual elements were concentrated upward or downward in the preeruptive magma chamber is revealed by enrichment factors illustrated in Figure 7, where elemental concentrations in early erupted pumice are divided by concentrations in late erupted felsite from the center of the dome. Those elements that were strongly enriched upward in the magma chamber include Li, Be, B, As, Sn, Sb, Cs, Ta, and W. Strongly depleted elements are Ti, Zn, Y, Zr, Ba, REE, Hf, Pb, and Th. Of particular importance are some elements that behave in opposite direction at Honeycomb Hills compared to enrichments and depletions in less evolved rhyolites such as the Bishop Tuff (Hildreth, 1979) or Twin Peaks, Utah (Crecraft et al., 1981). At those localities Y, Nb, and Th are enriched in evolved lavas. At Honeycomb Hills these elements are depleted in evolved samples because of precipitation of accessory mineral phases containing these elements in high abundance. Christiansen et al. (1986) report a similar de-

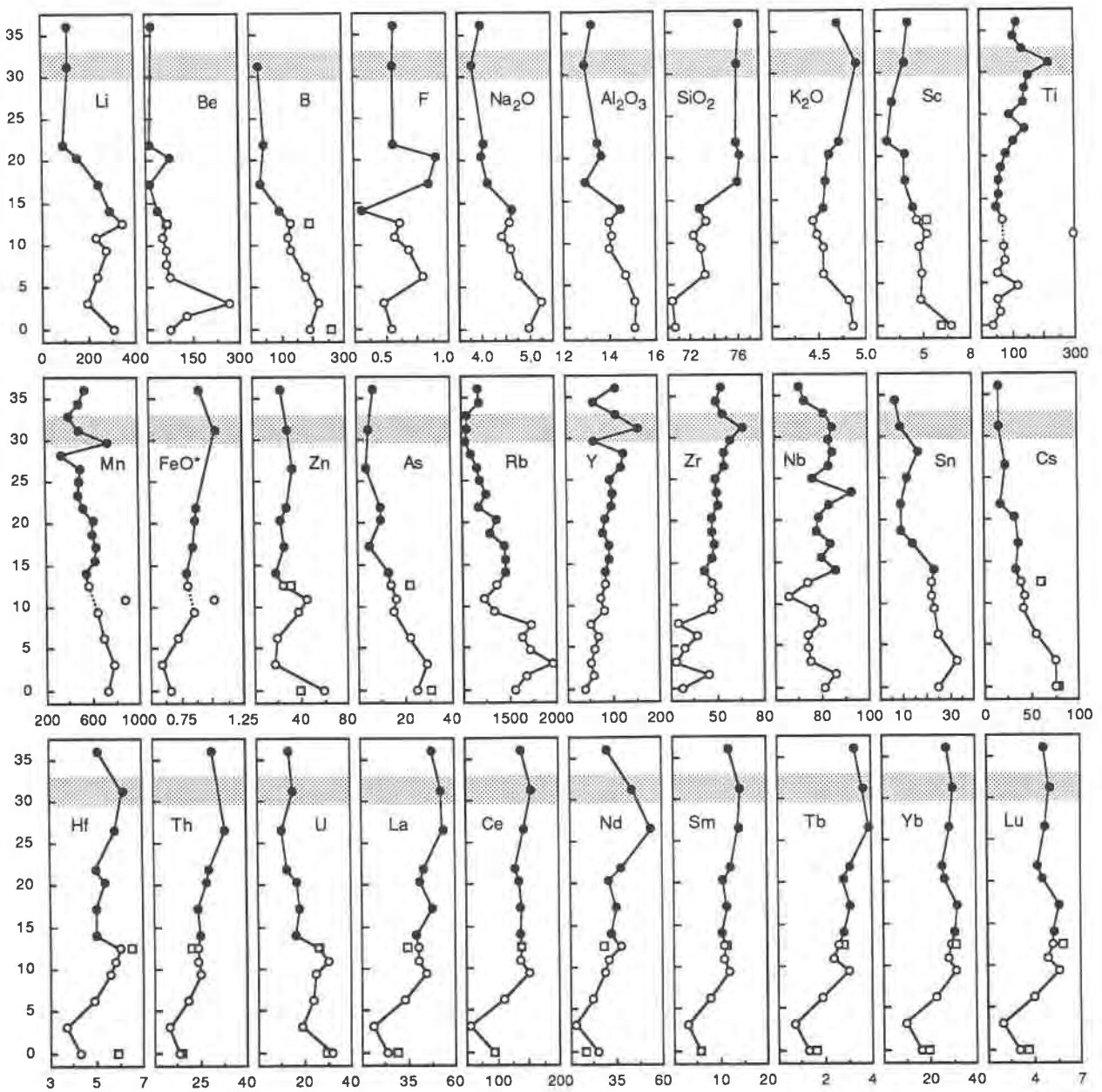

Fig. 6. Elemental composition vs. stratigraphic position. Elements are in ppm; oxides are in wt%. The shaded region is the approximate dome center and last erupted material. The y-axis is to scale in meters for the pyroclastic sequence but only shows relative position in the dome (above 12.5 m). Open circles are pumice. Open squares are glass separates, and filled circles are felsite.

pletion of Th and LREE during evolution of a F-rich granite from western Utah. Depletions of Nb and Y were not observed despite the presence of trace amounts of oxides rich in Nb and Ta.

The covariance of elements with differentiation is illustrated in Figure 8 where concentrations are plotted against abundance of Rb, which exhibits substantial and systematic variation throughout the eruptive sequence and serves as an index of differentiation. The figure illustrates the increase in abundance of Li, Be, Na, Al, As, Sn, and Cs with differentiation and the concomitant decline in concentrations of Si, Fe, Zr, and all the REE. The topaz-bearing xenolith is colinear with many elements, but there are notable exceptions such as FeO, Al_2O_3, and Zr.

There is no fractionation of light REE with respect to heavy REE as is commonly observed in silicic magma systems. All REE except Eu are depleted with differentiation. Chondrite normalized REE abundances produce a flat pattern (Fig. 9), characteristic of topaz rhyolites in general (Christiansen et al., 1986). These data also show

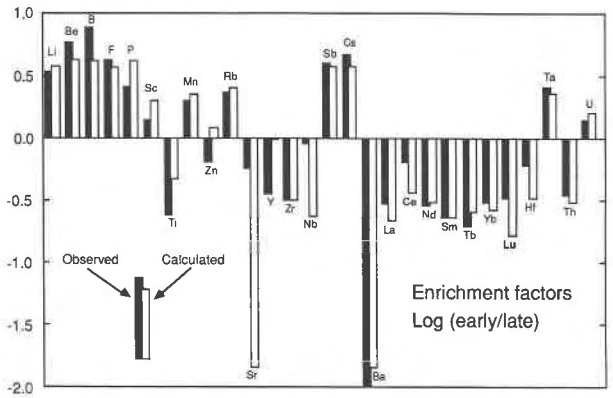

Fig. 7. Enrichment factors for the Honeycomb Hills rhyolite. Early material is sample 43, and late is sample 66 [except for Be = sample 56 (late), F = sample 32G (early), and Ta (1 early; 63 late)]. The comparison is for early erupted pumice vs. the central portion of the dome, i.e., the last erupted magma. Due to variability in Eu in pumice, an Eu factor has not been calculated. Calculated enrichment factors are based on 75% crystallization of phases in volume fraction abundances: quartz 0.330, plagioclase 0.305, sanidine 0.333, biotite 0.030, zircon 0.0003, thorite 0.000 045, fluocerite 0.0004, columbite 0.000 001, fergusonite 0.0005, and ishikawaite 0.00005.

greater variation in REE concentration within the 12.5 m pyroclastic sequence than within the entire volume of the dome.

Partition coefficients

Separates of the predominant mineral phases were analyzed for trace element concentrations (Table 2). Figure 3 illustrates the chondrite-normalized REE concentrations of these phases plus accessory phases analyzed by electron microprobe. Crystal-glass partition coefficients (K_d) have been calculated for each phase (Table 8). The inclusion of accessory minerals in phenocryst phases can produce significant and selective errors in calculated K_d values. Of particular concern is the common inclusion of zircon and monazite in biotite. For example, the separate of biotite sample 32 is apparently contaminated by zircon and monazite as revealed by high calculated partition coefficients for Hf, U, Th, and all REE. REE-bearing accessory phases were not observed in biotite from pumice sample 1, and we are confident that partition coefficients for that sample are appropriate. Zircon, thorite, monazite, and niobates are often included in topaz phenocrysts, and for this reason K_d values for topaz were not calculated. Megacrysts of topaz contain measurably lower concentrations of trace elements than phenocrysts, and they are devoid of inclusions; however, the composition of the melt from which they crystallized cannot be established. The source of the megacrysts is unknown. They may have grown in the Honeycomb Hills magma at an early stage and did not incorporate accessory phases that were yet to nucleate, or the megacrysts may be xenocrystal, having crystallized earlier in a pegmatite associated with the parent magma body of the Honeycomb Hills magma volume. The similarity in composition of megacrysts and phenocrysts strongly suggests that the two are genetically related and must have crystallized from the same or similar magmas. Accordingly, we attribute high trace element contents of topaz and other phenocrysts to inclusion of accessory phases, and we report here partition coefficients only for those phenocrysts that do not have suspiciously high trace element contents.

Biotite selectively incorporates Sc, Zn, Co, Rb, Ta, and Ba and has partition coefficients less than 1 for As, Cs, Hf, W, Au, Th, U, and all REE. None of the elements analyzed yielded partition coefficients greater than 1 for plagioclase, sanidine, or quartz, including Eu in feldspar. Accessory phases have extraordinarily high K_d values for selected elements. Zircon and thorite incorporate actinides and heavy REE. Niobates may incorporate Mn, Ta, and Sn and are strongly enriched in middle REE and HREE and individually enriched in Y, U, and Ce. Light REE are selectively incorporated in monazite and fluocerite. Monazite also contains substantial Th (12.5%). Th is partitioned more favorably than U in zircon, thorite, and monazite, whereas the opposite is true for niobates.

Physical parameters

Temperature

Equilibration temperatures were calculated for 64 pairs of plagioclase and alkali feldspar using the two-feldspar thermometer of Fuhrman and Lindsley (1988). These results are plotted against stratigraphic position in Figure 10. Temperatures are also tabulated in Table 3 for each feldspar pair reported there. To arrive at optimum convergence, the Fuhrman and Lindsley (1988) algorithm changed the measured feldspar compositions from 0 to 2 mol% in Ab and Or in both alkali feldspar and plagioclase. In all but three instances, An contents remained as analyzed. The adjustments are within the precision of the microprobe except for the positively adjusted Or content of 0.5 to 2.0 mol% (absolute) in plagioclase. The data indicate overall low temperatures from approximately 570 °C to 610 °C, with the suggestion amidst the scatter in the data of a small increase in temperature with order of eruption. These temperatures are slightly lower than the 600–640 °C range we reported previously (Congdon and Nash, 1988) as a result of reanalysis of the entire feldspar suite. It is not surprising that there is no large temperature gradient. First, the erupted volume is small, and second, it is crystal rich with phenocryst contents ranging from 10 to 48%. As Marsh (1981) has observed, the majority of crystallization takes place within a small temperature interval (primarily as the result of loss of latent heat of crystallization).

These temperatures are lower than those of common rhyolites but are within the range of experimental liquidi and solidi in volatile-rich silicic systems of extreme composition such as the rhyolite of Spor Mountain, Utah, and the glass from Macusani, Peru. At 200 MPa, the solidus for the Spor Mountain rhyolite extends from 650 to 500

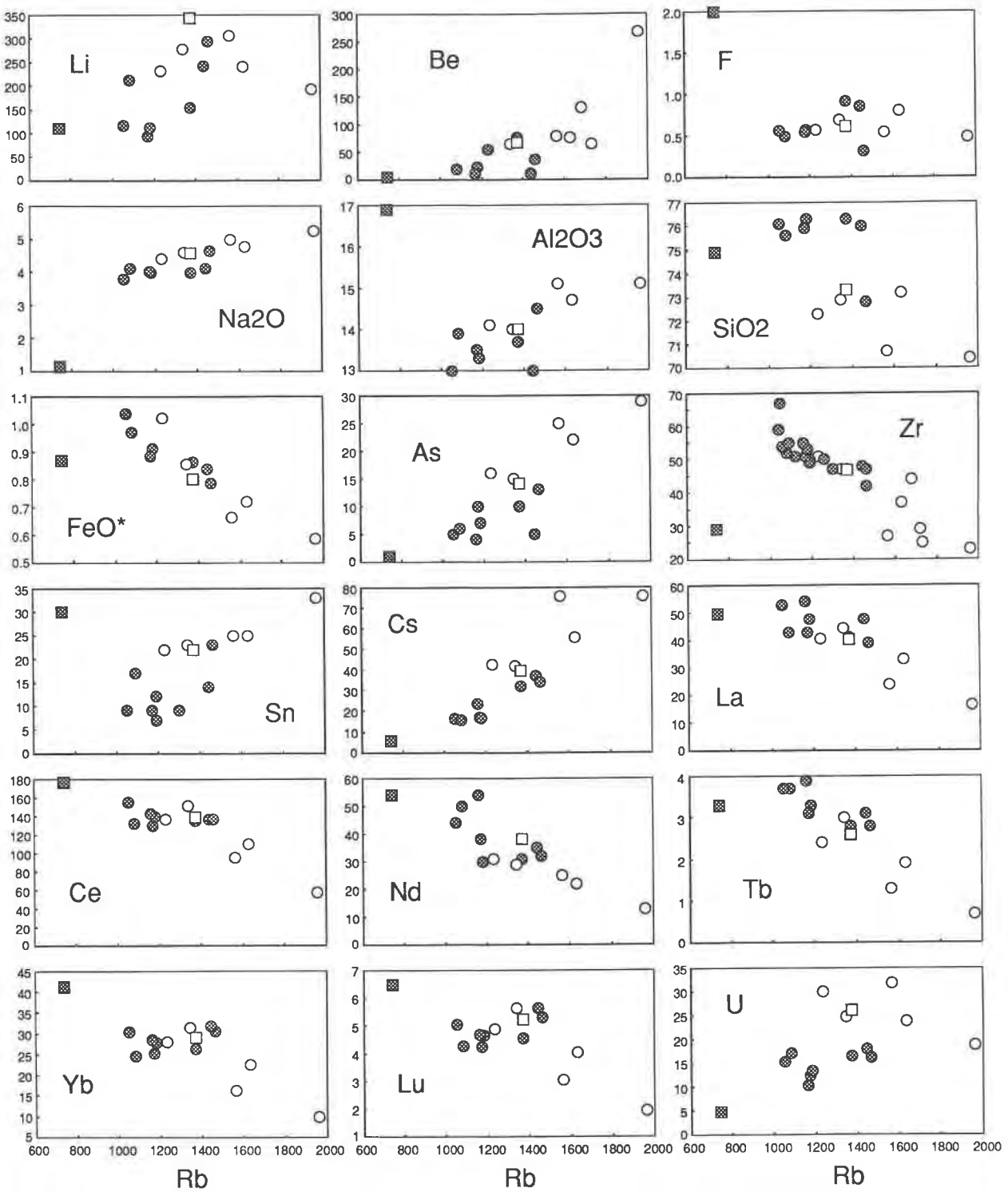

Fig. 8. Plots of selected elements vs. Rb. Elements are in ppm; oxides are in wt%. Open circles are pumice; closed circles are domal felsite. The open square is vitrophyre 32, and the solid square is xenolith 10.

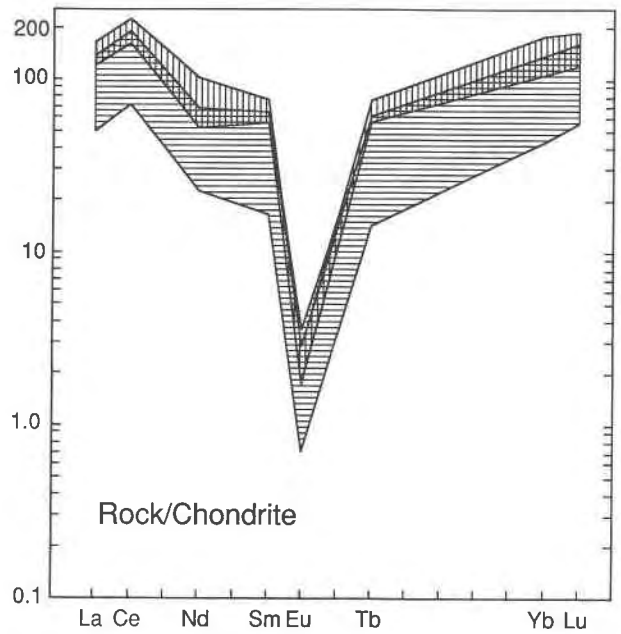

Fig. 9. Chondrite-normalized REE concentrations in pumice (horizontal pattern) and dome felsite (vertical pattern).

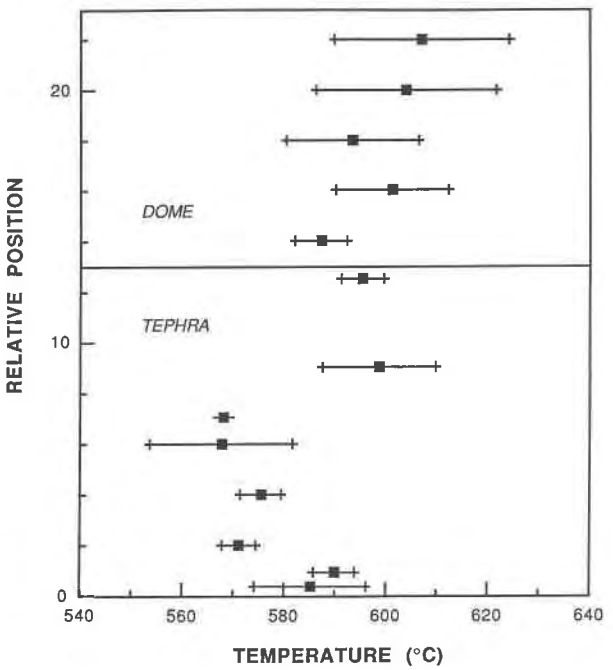

Fig. 10. Two-feldspar temperatures vs. stratigraphic position. Error bars represent 1 sd about the mean. The tephra section is shown to scale in meters.

°C depending on H_2O content (Webster et al., 1987), and the Macusanite H_2O-saturated solidus is in the region of 450 °C (London et al., 1988). Because we observe lavas with up to 50% crystals on the surface at the Honeycomb Hills, the magma had obviously not achieved its critical crystallinity where viscous flow to the surface was prohibited. This critical crystallinity occurs about midway between the liquidus and solidus (Marsh, 1981), and it is evident that the solidus for the Honeycomb Hills magma lies below 600 °C.

Oxygen fugacity

In the absence of coexisting titanomagnetite and ilmenite, f_{O_2} is calculated from measured Fe_2O_3/FeO in glass sample 32 by the method of Sack et al. (1980) as modified by Kilinc et al. (1983). Using an average temperature of 600 °C, an f_{O_2} of $10^{-17.4}$ bars is calculated for the vitrophyre, which places the magma 3 orders of magnitude above the fayalite-magnetite-quartz O buffer and on a trend consistent with f_{O_2}-temperature conditions for silicic ash-flow sheets from Nevada determined by Lipman (1971).

Water fugacity

The f_{H_2O} may be determined from coexisting biotite, sanidine, and magnetite as established experimentally by Wones and Eugster (1965). For the calculations presented here, we have adopted the equilibrium constant advocated by Hildreth (1977) as follows:

$$\ln f_{H_2O} = \frac{19973}{T} + \frac{0.00903}{T}(P - 1)$$
$$+ \ln a^{bi}_{KFe_3AlSi_3O_{10}(OH)_2} + \frac{1}{2}\ln f_{O_2}$$
$$- \ln a^{imt}_{Fe_2O_3} - \ln a^{san}_{KAlSi_3O_8}. \quad (1)$$

The activity for annite is given by the ideal mixing model:

$$a^{bi}_{KFe_3AlSi_3O_{10}(OH)_2} = ({}^{[12]}X_K)({}^{[6]}X_{Fe})^3(X_{OH})^2. \quad (2)$$

The activity of sanidine, Or_{65}, at 600 °C and 1000 bars is 0.75 (Carmichael et al., 1974). Reconnaissance microprobe scans of magnetite show negligible amounts of Ti, and thus the activity of magnetite is assumed to be unity. At 600 °C and an f_{O_2} of $10^{-17.4}$ bars, f_{H_2O} range from 1000 to 1135 bars in pumice and vitrophyre and from 133 to 200 bars in domal lavas (Table 4). These correspond to H_2O pressures of approximately 2000 and 220 bars, respectively (Burnham et al., 1969). The drop in f_{H_2O} between the pyroclastic sequence and the lavas is recorded in the increased F content and concomitant decrease in OH content of biotite.

Fluorine fugacity

Biotite phenocrysts in the pyroclastic sequence appear to have erupted rapidly, as they are homogeneous and show no evidence of reaction. Accordingly, they preserve the preeruptive H_2O/HF ratio of the magma. In contrast, biotite phenocrysts in subsequent erupted domal lavas are enriched in F and record the passive dewatering of the volume of magma that was erupted to form the dome.

TABLE 8. Crystal-liquid partition coefficients (K_d) for phenocryst and accessory phases

	Biotite		Plagio-clase	Sanidine	Quartz	Zircon	Thorite	Monazite	Fluo-cerite	Colum-bite	Fergu-sonite	Ishika-waite	Cerium niobate
Sc	19.6	21.6	0.03	0.03	0.02	—	—	—	—	—	—	—	—
Mn	—	—	—	—	—	—	—	—	—	100	—	28	30
Co	2.9	2.7	0.7	0.7	0.5	—	—	—	—	—	—	—	—
Zn	13	14	0.4	0.4	0.2	—	—	—	—	—	—	—	—
As	0.13	0.09	—	—	—	—	—	—	—	—	—	—	—
Rb	2.5	2.4	0.02	0.8	—	—	—	—	—	—	—	—	—
Y	—	—	—	—	—	—	—	—	—	—	—	—	—
Zr	—	—	—	—	—	8500	30	70	—	—	—	—	—
Nb	—	—	—	—	—	—	—	—	—	6400	4000	3700	3700
Sn	—	—	—	—	—	—	—	—	—	280	—	540	—
Sb	3.2	0.8	0.1	0.2	0.1	—	140	80	90	17	2200	100	150
Cs	0.56	0.53	0.01	0.03	0.01	—	—	—	—	—	—	—	—
Ba	1.2	2.1	—	0.13	0.13	—	—	—	—	—	—	—	—
Hf	0.88	—	0.22	0.14	0.12	7200	—	210	—	—	720	—	—
Ta	2.1	2.7	0.02	0.02	—	—	—	—	—	8700	390	1310	1270
W	0.7	1.0	—	—	—	—	—	—	—	—	—	—	—
Au	0.6	—	—	—	—	—	—	—	—	—	—	—	—
Th	0.58	—	0.29	0.12	0.1	250	19000	5030	—	—	610	2600	410
U	0.77	—	0.12	0.08	0.08	1400	8000	160	—	—	1100	7800	3100
La	0.49	—	0.99	0.41	0.07	—	32	2700	5400	—	17	7	74
Ce	0.59	—	0.42	0.12	0.04	—	12	1700	3000	—	43	25	790
Nd	0.33	—	0.32	0.11	—	—	58	3000	3400	—	530	225	113
Sm	0.62	—	0.14	0.04	0.04	—	106	1200	1600	—	910	250	230
Eu	0.95	—	—	0.48	0.26	—	—	14000	—	—	3000	—	—
Tb	0.50	—	0.11	0.04	0.07	125	—	93	—	—	2100	650	—
Yb	0.51	—	0.07	0.04	0.04	560	320	—	—	—	990	800	960
Lu	0.58	—	0.07	0.05	0.05	560	780	—	—	—	1000	600	1390

Note: Liquid composition is the glass, 32G.

The ratio f_{H_2O}/f_{HF}, which can be calculated from the analyzed biotite composition and experimental data of Munoz and Ludington (1974), is listed for representative phenocrysts in Table 4. The fugacity ratio in the pyroclastic sequence is about 750, whereas it is about 200 in the lavas of the dome. The significant drop in the ratio reflects preferential loss of H_2O from the melt to the vapor phase, resulting in a relative enrichment in F that has a fluid-melt partition coefficient less than one (Dingwell et al., 1985; Manning and Pichavant, 1988; Webster et al., 1987; London et al., 1988). HF fugacities range from 1.4 bars in pumice and vitrophyre to 0.9 bar in domal lavas (Table 4).

To assess the relative enrichment in F in micas of differing Fe/Mg ratios, Munoz (1984) formulated the F intercept value [IV(F)], which in effect compensates for Fe-F avoidance. High relative fugacities of F result in low intercept values. At the Honeycomb Hills, F intercept values range from 0.49 in pumice to −0.16 in the domal lavas. The latter are the lowest values yet recorded in either magmatic or hydrothermal environments. Munoz (1984) has summarized F intercept values from a variety of settings, including Sierran granites (2.1), rhyolites (2.0–2.3), Pikes Peak granite (1.5), Santa Rita porphyry copper deposit (2.2–1.9), and Henderson porphyry molybdenum deposit (0.76–0.68). The only value within the range of the Honeycomb Hills is 0.34 for biotite associated with Sn mineralization in Nigeria. It is evident from these comparisons that the Honeycomb Hills represents a magmatic system that is extraordinarily enriched in F relative to H_2O.

Viscosity

Viscosities of dry silicic magmas are of the order of 10^{12} poise at the liquidus. If dry, the Honeycomb Hills magma probably would not have erupted to the surface. H_2O is effective in reducing the viscosity of magmas, and the addition of 5 wt% H_2O to a dry granitic melt serves to reduce the viscosity by 6 orders of magnitude. F serves a similar role in reducing the viscosity as well as the melting temperature of silicic magmas (Mysen and Virgo, 1985; Dingwell et al., 1985; Rabinovich, 1983; Wyllie and Tuttle, 1961). Dingwell et al. (1985) determined that the reduction in viscosity due to added F is greatest for high-silica rhyolites. A rhyolite melt with 75% SiO_2 is reduced in viscosity from 10^8 poise to about 10^5 poise with the addition of approximately 3 wt% F at 1000 °C. The effects of H_2O and F appear to be additive, and 1 mol of F has at least the equivalent effect as 1 mol of H_2O (Dingwell et al., 1985). Recently, Dingwell (1987) has shown that there is a negative deviation from the additivity of H_2O and F, which further reduces viscosity in albite melts. Extrapolation of the high-temperature experimental data at 7 kbar to the temperature of the Honeycomb Hills magma suggests that viscosities could be reduced by an additional order of magnitude over the additive properties of the 1:1 molar experimental concentrations of 5.58% H_2O and 11.7% F. At lower pressure and with substantially less F than in the experiment, this synergistic effect will be less in the Honeycomb Hills magma but may lower viscosities slightly from those calculated below.

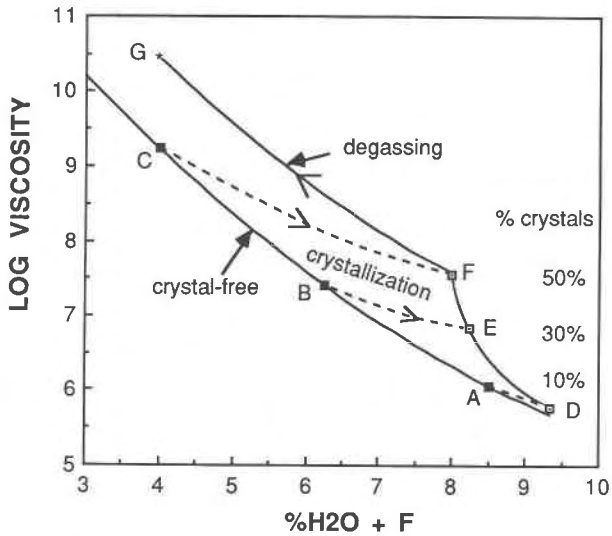

Fig. 11. Viscosity (poise) vs. total H_2O + F content of the melt. See text for discussion.

Analyses of melt inclusions in quartz phenocrysts by secondary ion mass spectrometry and electron microprobe indicate H_2O contents of 4.5–5.5 wt% in the upper part of the preeruptive magma body (Gavigan et al., 1989). Melt inclusions in domal lavas have H_2O contents ranging from 1 to 3 wt%. Similarly, F contents in melt inclusions decline from 3.5% in early erupted material to 2% in domal lavas. Accordingly, the total H_2O plus F content in the upper portion of the magma chamber was about 8–9 wt%. In the mass of the magma that ultimately gave rise to the domal lavas, the total H_2O plus F content was approximately 4 wt%. Assuming that F has an effect equivalent to H_2O in reducing viscosity, these volatile contents provide viscosities for a crystal-free melt of $10^{6.1}$ and $10^{9.3}$ poise, respectively (Shaw, 1965). The rheological properties of the magma will be further modified by the effects of crystallization and degassing, which are considered below.

Crystallinity

In general, a crystal-free rhyolite melt above its liquidus exhibits pseudoplastic behavior (Spera et al., 1982). That is, at low strain rates the behavior is Newtonian, but at high strain rates viscosity has a negative deviation from linearity. However, magmas are rarely above their liquidi, and in magmas with low volatile contents, crystallization tends to increase viscosity rapidly; when phenocryst contents exceed 50–60%, noncreep flow is not possible. A dramatic change in viscosity should occur at a critical crystallinity where crystal interference will cause the whole mass to lock up and freeze at depth (Marsh, 1981). A tradeoff does exist, however, because high crystal content will cause a magma to cool more slowly because of the latent heat of crystallization, and a magma that retains its heat better will remain fluid longer. Marsh (1981) places the critical crystallinity at about 55–60% in andesites and basalts; he suggests that it is substantially lower in more viscous, silicic magmas, perhaps as low as 20% in anhydrous melts and 25–35% in "moist" magmas. In the Honeycomb Hills rhyolites, crystallinities of 50% are approached; these levels require high volatile contents to provide sufficiently low viscosities for flow to the surface.

The effect of crystallization on the rheology of the Honeycomb Hills magma may be evaluated using Roscoe's (1953) formula:

$$\mu = \mu_L(1 - RX)^{-2.5} \quad (5)$$

where μ is the viscosity of the liquid plus crystals, μ_L is the viscosity of the crystal-free liquid, and X is the fraction of crystals. R is a constant, with a value that is the inverse of the critical packing density of crystals, at which the mass cannot flow. To allow movement at constant volume, a random packing density is assumed. For spheres this is 0.62, and $R = 1/0.62 = 1.61$. For an increase in phenocryst abundance from 10% in early erupted pumice to 50% in domal lavas, the effect in an anhydrous melt is to increase viscosities by over an order of magnitude in the crystal-rich magma. Creep effects were unimportant because deformed phenocrysts do not occur.

However, there is an opposing effect in volatile-rich magmas because of the concentration of volatile constituents in the residual melt as crystallization proceeds. Crystallization of 50% of quartz and feldspar serves to double the concentration of volatiles in the melt, which reduces the effective viscosity by an amount significantly greater than the increase produced by crystals alone. The net effect is that crystallization in volatile-rich systems reduces the effective viscosity of the magma as long as the volatiles are retained in the magma. This effect is illustrated in Figure 11. Line AC is the viscosity of crystal-free Honeycomb Hills melt at 600 °C as a function of total volatile content (Shaw, 1972), assuming that F has the equivalent effect of H_2O in reducing the viscosity of silicate melts. Paths AD, BE, and CF illustrate the reduction in viscosity with crystallization of 10–50% from magma volumes with differing initial volatile contents as recorded by melt inclusions. The decline in viscosity of the magma results from increased volatile concentrations in residual liquids, whereas the deviation upward from the crystal-free viscosity curve results from increased crystal content of the magma. The curve DF represents an approximate preeruptive gradient in viscosity from the earliest erupted pumice, with 10% crystals (D) to the magma volume producing the domal lavas with 50% phenocrysts (F). Magma with up to 30% crystals vesiculated rapidly, fragmented, and was erupted explosively to form the pyroclastic sequence. The more crystal-rich magma degassed passively on route to the surface, with preferential loss of H_2O over F to the fluid phase that resulted in increased viscosity along an approximate path represented by FG. The path FG represents a minimum slope, because degassing on route to the surface promotes crystallization that in turn raises viscosity. This effect was

probably minimal because of the high proportion of F retained by the melt. It seems probable that the eruption ceased when crystallinity in either the conduit or upper reaches of the magma chamber achieved a critical value beyond which flow to the surface was prohibited, regardless of the volatile content of the interstitial melt. At the Honeycomb Hills, this value is about 50% crystals, which is the phenocryst content of felsite in the conduit.

The magma at point F contains 4% H_2O as well as 4% F. In the Harding pegmatite, saturation at 4% H_2O occurs at 1000 bars pressure (Burnham and Jahns, 1962). In a Spor Mountain vitrophyre, which is compositionally similar to Honeycomb Hills lavas, H_2O saturation occurs experimentally at about 3.3% H_2O at 500 bars and 4.5% H_2O at 1000 bars (Webster et al., 1987). Accordingly, we estimate that passive degassing of the magma began at pressures slightly less than 1000 bars or at depths of 2 to 3 km. Despite the loss of H_2O, the presence of substantial F kept viscosities sufficiently low to permit flow of the magma to the surface. Furthermore, if the negative deviation from the additive properties of H_2O and F observed in albite melts (Dingwell, 1987) occurs in natural silicic magmas, then an increase in the F/H_2O ratio toward a 1:1 molar ratio will retard the rate of increase in viscosity that inevitably accompanies degassing. Ultimately, much of the F was lost during crystallization of the groundmass of the domal lavas.

Chemical evolution

Fractionation model

The data in Figures 5 and 6 illustrate that there are systematic variations in chemical composition with respect to sequence of eruption and, by inference, to position in the preeruptive magma chamber. Although the lavas of the Honeycomb Hills share similar characteristics of enrichment factors with high-silica rhyolites, there are distinct differences including depletion in Y, Nb, Th, and all the REE. These elements are abundant in accessory phases including several niobates, zircon, thorite, and fluocerite. The presence of these particular phases and the uncharacteristic depletion of some elements strongly suggest that the concentrations of many trace elements in silicic magmas are controlled by crystal-liquid equilibria and not by diffusive properties of the melt alone. Some elements such as Sb, which are incompatible in all phases, are simply enriched in residual melts.

The enrichment and depletion patterns observed (Fig. 7) can be reproduced by Rayleigh fractionation of the phenocryst phases using partition coefficients measured for phenocrysts at the Honeycomb Hills. Because of the large number of phases present, the model has considerable latitude and is only permissive evidence that fractionation is a possible mechanism for the chemical diversity observed. The optimum result is obtained for crystallization of 75% of the initial magma volume: the correspondence of the model results with observation is illustrated in Figure 7. The abundance of phases removed in the model is given by Congdon and Nash (1988, Fig. 1). The role of accessory phases is evident where thorite removes Th, whereas U is enriched in residual liquids. Similarly, Nb and Y are removed from the magma by precipitation of Ta-poor niobates, resulting in enrichment in Ta.

More than 75% crystallization is required to explain extraordinary enrichments in B, Be, and, to a lesser extent, F, Li, and Cs. It is possible that these elements are depleted in the domal lavas as a result of loss to the fluid phase during degassing, so that the actual enrichments produced by crystallization may not be as great as they appear. B has a positive fluid-melt partition coefficient (Pichavant, 1981, 1987; London et al., 1988), and Webster et al. (1987) have shown experimentally that Li, Be, B, and Cs are partitioned preferentially into the fluid phase in F-rich silicic melts. Accordingly, these relative enrichments may not reflect preeruptive gradients but are the result of the eruption itself.

The variation in major elements illustrated in Figure 5 is consistent with the differentiation of the early erupted magma volume in response to the crystallization of quartz and feldspar, resulting in increased F and H_2O contents in residual melts. The data are also consistent with F contents of up to 3% in the early erupted magma.

As noted previously, composition varies more in the pyroclastic sequence than in the domal lavas. This may be due in part to the ability to separate liquids from crystals more readily in crystal-poor systems than in crystal-rich systems where crystal movement is more inhibited or the extraction of interstitial melt is more tortuous. We advocate phase separation of a buoyant, volatile enriched melt at the crystallizing margin of the magma chamber and its subsequent accumulation as a density stratified melt in the uppermost portion of the magma chamber. It is evident that accessory phases are instrumental in controlling many trace element abundances. Fractionation of these phases by gravitational settling cannot be effective because of their small size. Separation by inclusion in larger phenocryst phases is possible; however, only biotite and topaz commonly contain accessory inclusions, and they themselves are not abundant. For this reason, we prefer a mechanism of multiphase crystallization at the margins of the chamber, accompanied by buoyant separation of the residual melt fraction.

Petrogenesis

Aside from their porphyritic texture, the lavas of the Honeycomb Hills possess the chemical and mineralogical characteristics of a rare element pegmatite. These bodies are typically enriched in Be, Li, Rb, Cs, Ta, Nb, and Sn, and the concentrations of these elements at the Honeycomb Hills fall within the range reported for rare element pegmatites (Černý, 1982). For example, Sn is present in concentrations up to 33 ppm at the Honeycomb Hills; granites with Sn mineralization are reported to contain 16 to 32 ppm Sn, whereas 3 ppm is usual for common granite (Wedepohl, 1970). REE-bearing accessory phases

such as fluocerite and niobates are common in rare element pegmatites (Henderson, 1984). Pegmatites commonly contain two micas. Muscovite phenocrysts are rare in volcanic rocks, and at the Honeycomb Hills topaz may proxy for muscovite by the following reaction, which has a positive molar volume change and would be favored by lower pressures:

$$\underset{\text{muscovite}}{KAl_2AlSi_3O_{10}(OH,F)_2} + \underset{\text{quartz}}{SiO_2} = \underset{\text{topaz}}{Al_2SiO_4(OH,F)_2} + \underset{\text{sanidine}}{KAlSi_3O_8}.$$

Domal lavas contain pegmatite xenoliths as well as megacrysts of sanidine, topaz, and biotite up to 8 cm in diameter. All these characteristics indicate that the lavas of the Honeycomb Hills were erupted from a pegmatitic magma.

The origin of the pegmatitic magma remains more enigmatic. We envision it arose by prolonged differentiation within a cupola in the upper reaches of a granitic magma whose own origin provided modest enrichments in rare elements and F. The most likely source region for such a magma lies in the Proterozoic continental crust. Christiansen and Lee (1986) surveyed the distribution of F in granitoids of the western United States and demonstrated that the highest F contents were in Precambrian granitoids. We agree with their suggestion that F-rich magmas could be produced from these protoliths by anatexis of Precambrian terrains of Protoerozoic age in which the F is derived from the breakdown of biotite whose F contents have been enriched through one or more prior thermal events.

Acknowledgments

Support for this study was provided by National Science Foundation grant EAR-8720627 to W.P.N. and the Mineral Leasing Fund of the University of Utah. The Cameca electron microprobe was purchased with funds from the National Science Foundation (grant EAR-8618101) and the University of Utah. The manuscript was substantially improved by the thorough reading and many helpful comments of Eric H. Christiansen.

References cited

Bacon, C.R., Macdonald, R., Smith, R.L., and Baedecker, P.A. (1981) Pleistocene high-silica rhyolites of the Coso volcanic field, Inyo County, California. Journal of Geophysical Research, 66, 10223–10241.

Burnham, C.W., and Jahns, R.H. (1962) A method for determining the solubility of water in silicate melts. American Journal of Science, 260, 721–745.

Burnham, C.W., Holloway, J.R., and Davis, N.F. (1969) Thermodynamic properties of water to 1000 °C and 10,000 bars. Geological Society of America Special Paper 132, 96 p.

Carmichael, I.S.E., Turner, F.J., and Verhoogen, J. (1974) Igneous petrology, 739 p. McGraw-Hill, New York.

Černý, P. (1982) Petrogenesis of granitic pegmatites. In P. Černý, Ed., Granitic pegmatites in science and industry. Mineralogical Society of Canada Short Course Handbook, 8, 405–462.

Christiansen, E.H., and Lee, D.E. (1986) Fluorine and chlorine in granitoids from the Basin and Range province, western United States. Economic Geology, 81, 1484–1494.

Christiansen, E.H., Bikun, J.V., Sheridan, M.F., and Burt, D.M. (1984) Geochemical evolution of topaz rhyolites from the Thomas Range and Spor Mountain, Utah. American Mineralogist, 69, 223–236.

Christiansen, E.H., Sheridan, M.F., and Burt, D.M. (1986) The geology and geochemistry of Cenozoic topaz rhyolites from the western United States. Geological Society of America Special Paper 205, 82 p.

Congdon, R.D., and Nash, W.P. (1988) High-fluorine rhyolite: An eruptive pegmatite magma at the Honeycomb Hills, Utah. Geology, 16, 1018–1021.

Crecraft, H.R., Nash, W.P., and Evans, S.H., Jr. (1981) Late Cenozoic volcanism at Twin Peaks, Utah: Geology and petrology. Journal of Geophysical Research, 86, 10303–10320.

Deer, W.A., Howie, R.A., and Zussman, J. (1962) Rock-forming minerals, vol. 3, 270 p. Wiley, New York.

Dingwell, D.B. (1987) Melt viscosities in the system $NaAlSi_3O_8$-H_2O-F_2O_{-1}. Geochemical Society Special Publication No. 1, 423–432.

Dingwell, D.B., Scarfe, C.M., and Cronin, D.J. (1985) The effect of fluorine on viscosities in the system Na_2O-Al_2O_3-SiO_2: Implications for phonolites, trachytes and rhyolites. American Mineralogist, 70, 80–87.

Drake, M.J., and Weill, D.F. (1975) Partition of Sr, Ba, Ca, Y, Eu^{+2}, Eu^{+3}, and other REE between plagioclase feldspar and magmatic liquid: An experimental study. Geochimica et Cosmochimica Acta, 39, 669–712.

Fuhrman, M.L., and Lindsley, D.H. (1988) Ternary feldspar modeling and thermometry. American Mineralogist, 73, 201–215.

Gavigan, T.H., Nash, W.P., and Webster, J.D. (1989) Preeruptive gradients in silicic magma as recorded by melt inclusions. Eos, 70, 1417.

Hagstrum, J.T., and Gans, P.B. (1989) Paleomagnetism of the Oligocene Kalamazoo Tuff: Implications for middle Tertiary extension in east central Nevada. Journal of Geophysical Research, 94, 1827–1842.

Henderson, P. (1984) Rare earth element geochemistry, 510 p. Elsevier, New York.

Hildreth, E.W. (1977) The magma chamber of the Bishop Tuff: Gradients in temperature, pressure, and composition, 328 p. Ph.D. thesis, University of California, Berkeley, California.

——— (1979) The Bishop Tuff: Evidence for the origin of compositional zonation in silicic magma chambers. Geological Society of America Special Paper 180, 43–75.

Hintze, L.F. (1988) Geologic history of Utah. Brigham Young University Geology Studies Special Publication 7, 202 p.

Hogg, N.C. (1972) Shoshonitic lavas in west-central Utah. Brigham Young University Geology Studies, 10, 133–184.

Kilinc, A., Carmichael, I.S.E., Rivers, M.L., and Sack, R.O. (1983) The ferric-ferrous ratio of natural silicate liquids equilibrated in air. Contributions to Mineralogy and Petrology, 83, 136–140.

Kovalenko, V.I. (1973) Distribution of fluorine in a topaz-bearing quartz keratophyre (ongonite) and mobility of fluorine in quartz melts. Geochemistry International, 10, 41–49.

Kovalenko, V.I., and Kovalenko, N.I. (1976) Ongonites (topaz-bearing quartz keratophyre)—Subvolcanic analogue of rare metal Li-F granites. Nauka Press, Moscow (in Russian).

Kovalenko, V.I., Kuz'mun, M.I., Antipin, V.S., and Petrov, L.L. (1971) Topaz-bearing quartz keratophyre (ongonite), a new variety of subvolcanic igneous vein rock. Doklady Akademii Nauk SSSR, Earth Sciences Section, 199, 132–135.

Kovalenko, V.I., Antipin, V.S., Konusova, V.V., Smirnova, Ye.V., Petrov, L.L., Vladykin, N.V., Kuznetsova, A.I., Kostukova, Ye.S., and Pisarskaya, V.A. (1977) Partition coefficients of fluorine, niobium, tantalum, lanthanum, ytterbium, tin and tungsten in ongonite. Doklady Akademii Nauk SSSR, Earth Sciences Section, 233, 203–205.

Lindsey, D.A. (1977) Epithermal beryllium deposits in water-laid tuff, western Utah. Economic Geology, 72, 219–232.

Lipman, P.W. (1971) Iron-titanium oxide phenocrysts in compositionally zoned ash-flow sheets from southern Nevada. Journal of Geology, 79, 438–448.

London, D., Hervig, R.L., and Morgan, G.B., IV (1988) Melt-vapor solubilities and elemental partitioning in peraluminous granite-pegmatite systems: Experimental results with Macusani glass at 200 MPa. Contributions to Mineralogy and Petrology, 99, 360–373.

Manning, D.A.C. (1981) The effect of fluorine on liquidus phase relationships in the system qz-ab-or with excess water at 1 kb. Contributions to Mineralogy and Petrology, 76, 206–215.

Manning, D.A.C., and Pichavant, M. (1988) Volatiles and their bearing

on the behaviour of metals in granitic systems. Canadian Institute of Mining and Metallurgy Special Volume 39, 13–24.

Marsh, B.D. (1981) On the crystallinity, probability of occurrence and rheology of lava and magma. Contributions to Mineralogy and Petrology, 78, 85–98.

McAnulty, W.N., and Levinson, A.A. (1964) Rare alkali and beryllium mineralization in volcanic tuffs, Honey Comb Hills, Juab County, Utah. Economic Geology, 59, 768–774.

Munoz, J.I. (1984) F-OH and Cl-OH exchange in micas with applications to hydrothermal ore deposits. In Mineralogical Society of America Reviews in Mineralogy, 13, 469–493.

Munoz, J.I., and Ludington, S.D. (1974) Fluoride-hydroxyl exchange in biotite. American Journal of Science, 274, 396–413.

Mysen, B.O., and Virgo, D. (1985) Structure and properties of fluorine-bearing aluminosilicate melts: The system SiO_2-F at 1 atm. Contributions to Mineralogy and Petrology, 91, 205–220.

Nash, W.P., and Crecraft, H.R. (1985) Partition coefficients for trace elements in silicic magmas. Geochimica et Cosmochimica Acta, 49, 2309–2322.

Pichavant, M. (1981) An experimental study of the effect of boron on a water saturated haplogranite at 1 kbar pressure. Geological applications. Contributions to Mineralogy and Petrology, 76, 430–439.

——— (1987) Effects of B and H_2O on liquidus phase relations in the haplogranite system at 1 kbar. Bulletin Mineralogique, 106, 201–211.

Pichavant, M., and Manning, D.A.C. (1984) Petrogenesis of tourmaline granites and topaz rhyolites; the contribution of experimental data. Physics of the Earth and Planetary Interiors, 35, 31–50.

Pichavant, M., Herrera, J.V., Boulmier, S., Briqueu, L., Joron, J.-L., Juteau, M., Marin, L., Michard, A., Shepard, S.M.F., Treuil, M., and Vernet, M. (1987) The Macusani glasses, SE Peru: Evidence of chemical fractionation in peraluminous magmas. Geochemical Society Special Publication, 1, 359–373.

Rabinovich, E.M. (1983) On the structural role of fluorine in silicate glasses. Physics and Chemistry of Glasses, 24, 54–56.

Roscoe, R. (1953) Suspensions. In J.J. Hermans, Ed., Flow properties of disperse systems, p. 1–38. North Holland, Amsterdam.

Sack, R.O., Carmichael, I.S.E., Rivers, M., and Ghiorso, M.S. (1980) Ferric-ferrous equilibria in natural silicate liquids at 1 bar. Contributions to Mineralogy and Petrology, 75, 369–376.

Shaw, H.R. (1965) Comments on viscosity, crystal settling, and convection in granitic magmas. American Journal of Science, 263, 120–152.

——— (1972) Viscosities of magmatic silicate liquids: An empirical method of prediction. American Journal of Science, 272, 870–893.

Spera, F.J. (1984) Some numerical experiments on the withdrawal of magma from crustal reservoirs. Journal of Geophysical Research, 89, 8222–8236.

Spera, F.J., Yuen, D.A., and Kirschvink, S.J. (1982) Thermal boundary layer convection in silicic magma chambers: Effects of temperature-dependent rheology and implications for thermogravitational chemical fractionation. Journal of Geophysical Research, 87, 8755–8767.

Spera, F.J., Yuen, D.A., Greer, J.C., and Sewell, G. (1986) Dynamics of magma withdrawal from stratified magma chambers. Geology, 14, 723–726.

Turley, C.H., and Nash, W.P. (1980) Volcanism in western Juab and Millard counties, Utah. Utah Geological and Mineral Survey Special Studies, 52, 1–33.

Webster, J.K.D., Holloway, J.R., and Hervig, R.L. (1987) Phase equilbria of a Be, U and F enriched vitrophyre from Spor Mountain, Utah. Geochimica et Cosmochimica Acta, 51, 389–402.

Wedepohl, K.H. (1970) Tin. Handbook of geochemistry. Springer-Verlag, New York.

Wones, D.R., and Eugster, H.P. (1965) Stability of biotite: Experiment, theory and application. American Mineralogist, 50, 1228–1272.

Wyllie, P.J., and Tuttle, O.F. (1961) Experimental investigation of silicate systems containing two volatile components—part II. The effects of NH_3 and HF, in addition to H_2O on the melting temperatures of albite and granite. American Journal of Science, 259, 128–143.

Manuscript received March 12, 1990
Manuscript accepted April 15, 1991